Atmos. Meas. Tech. Discuss., https://doi.org/10.5194/amt-2017-382
Manuscript under review for journal Atmos. Meas. Tech.
Discussion started: 10 January 2018

Atmospheric Measurement Techniques Discussions

The influence of instrumental line shape degradation on NDACC gas retrievals

Youwen Sun[1, 3)+], Mathias Palm [2)+], Cheng Liu [3, 4, 1)*], Frank Hase [5)], David Griffth [6)], Christine Weinzierl [2)], Christof Petri [2)], Wei Wang [1)], and Justus Notholt [2)]

(1 *Key Laboratory of Environmental Optics and Technology, Anhui Institute of Optics and Fine Mechanics, Chinese Academy of Sciences, Hefei 230031, China*)

(2 *University of Bremen, Institute of Environmental Physics, P. O. Box 330440, 28334 Bremen, Germany*)

(3 *Center for Excellence in Urban Atmospheric Environment, Institute of Urban Environment, Chinese Academy of Sciences, Xiamen 361021, China*)

(4 *University of Science and Technology of China, Hefei, 230026, China*)

(5 *Karlsruhe Institute of Technology (KIT), Institute for Meteorology and Climate Research (IMK-ASF), Karlsruhe, Germany*)

(6 *School of Chemistry, University of Wollongong, Northfields Ave, Wollongong, NSW, 2522, Australia*)

+These two authors contributed equally to this work

Abstract:

Instrumental line shape (ILS) degradation can cause significant biases between global FTIR (Fourier transform infrared) networks if not properly treated. Currently, how ILS degradation influences the global NDACC (Network for Detection of Atmospheric Composition Change) gases retrieval and how much ILS deviation is acceptable for each NDACC gas are still not fully quantified. We simulated ILS degradations with respect to typical types of misalignment, and compared their influence on each NDACC gas. The sensitivities of total column, root mean square of fitting residual (RMS), total random uncertainty, total systematic uncertainty, total uncertainty, degrees of freedom for signal (DOFs), and profile with respect to different levels of ILS degradation for all current NDACC gases, i.e., O_3, HNO_3, HCl, HF, $ClONO_2$, CH_4, CO, N_2O, C_2H_6, and HCN, were investigated. The influence of an imperfect ILS on NDACC gases retrieval were assessed, and the consistency under different meteorological conditions and solar zenith angles (SZA) were examined.

Correspondence to: Cheng Liu (chliu81@ustc.edu.cn)

Atmos. Meas. Tech. Discuss., https://doi.org/10.5194/amt-2017-382
Manuscript under review for journal Atmos. Meas. Tech.
Discussion started: 10 January 2018

Atmospheric Measurement Techniques Discussions

The study concluded that the influence of ILS degradation can be approximated by the linear sum of individual modulation efficiency (ME) amplitude influence and phase error (PE) influence. The PE influence is of secondary importance compared with the ME amplitude influence. For total column retrieval, the stratospheric gases are more sensitive to ILS degradation than the tropospheric gases. For profile retrieval, the positive ME has more influence on tropospheric gases than the stratospheric gases. In contrast, the negative ME has more influence on stratospheric gases than the tropospheric gases. In order to suppress the influence on total column for $ClONO_2$ and other NDACC gases within 10% and 1%, respectively, the permitted maximum ILS degradation for each NDACC gas was deduced (summarized in Table 5).

Key words: NDACC, FTIR, Instrumental line shape, Profile retrieval

1 Introduction

In order to achieve consistent results between different FTIR (Fourier transform infrared) sites, the TCCON (Total Carbon Column Observing Network, http://www.tccon.caltech.edu/) and NDACC (Network for Detection of Atmospheric Composition Change, http://www.ndacc.org/) have developed strict data acquisition and retrieval methods to minimize site to site differences (Hase et al., 2012; Wunch et al., 2010 and 2011; Washenfelder, 2006; Messerschmidt et al., 2010; Kurylo, 1991; Davis et al., 2001; Schneider, et al.,2008; Kohlhepp et al., 2011; Hannigan et al., 2009; Vigouroux et al., 2008 and 2015). Interferograms are acquired with similar instruments operated with common detectors, acquisition electronics and/or optical filters. These interferograms are first converted to spectra and then these spectra are analyzed using dedicated processing algorithms, i.e., GFIT, PROFFIT or SFIT (Wunch et al., 2010 and 2015; Hase et al., 2006; Hannigan and Coffey, 2009). Typically, the TCCON network only uses the Bruker 125HR instruments (http://www.tccon.caltech.edu/; https://www.bruker.com/) with specified settings (entrance aperture, amplification of the detected signal). In the NDACC network, other instruments are used as well, e.g., the Bruker M series, a BOMEM DA8 in

Atmos. Meas. Tech. Discuss., https://doi.org/10.5194/amt-2017-382
Manuscript under review for journal Atmos. Meas. Tech.
Discussion started: 10 January 2018

Atmospheric Measurement Techniques Discussions

Toronto, Canada and a self-built spectrometer in Pasadena, USA (http://www.ndacc.org/; https://www.bruker.com/). FTIR spectrometers are highly precise and stable measurement devices and the instrumental line shapes (ILSs) not far from the theoretical limit if carefully aligned. However, their alignment can change abruptly as a consequence of operator intervention or drift slowly due to mechanical degradation over time (Olsen et al., 2004; Duchatelet et al., 2010; Hase et al., 2012; Feist et al., 2016). Moreover, the NDACC observation may change the entrance field stop size if incident radiation changes. This practice may introduce a dependency of the instrument alignment status on the optical settings because the mechanical errors between different field stops may be non-negligible and inconsistent (Sun et al., 2017). Biases between sites would arise if all these misalignments are not properly characterized.

The TCCON network assumes an ideal ILS in spectra retrieval, and the maximum ILS degradation is prescribed as 5% for the modulation efficiency (ME) amplitude (Wunch et al., 2011 and 2015). This assumption still holds within the required accuracy of the results. In the NDACC gases retrieval, the ILS can be assumed as ideal if spectrometer is well aligned, or if misalignment exists, described by LINEFIT results derived from dedicated cell measurements or retrieved together with the gas profile from an atmospheric spectrum using a polynomial (Vigouroux et al., 2008 and Vigouroux et al., 2015). How these ILS treatments influence the NDACC gases retrieval and how much ILS deviation from unity is acceptable for each NDACC gas if an ideal line shape is assumed are still not fully quantified, and it may be better to assume an ideal ILS. The practice of co-retrieving ILS parameters from atmospheric spectra without dedicated cell measurements is not to be recommended because the observed shapes of spectral lines are exploited primarily for inferring the vertical distribution of the trace gases, the ILS and the trace gas profiles have similar effects on the line shape, i.e., changing the shape and width of the line. Overlapping lines, i.e., due to interfering gases may introduce an asymmetry in the absorption lines which may be undistinguishable from an ILS phase deviation.

This paper investigates the influence of ILS degradation on NDACC gas

Atmos. Meas. Tech. Discuss., https://doi.org/10.5194/amt-2017-382
Manuscript under review for journal Atmos. Meas. Tech.
Discussion started: 10 January 2018

Atmospheric Measurement Techniques Discussions

retrievals and deduces the maximum ILS deviations allowable for suppressing the influence within a specified acceptable ranges.

2 Characteristics of ideal and imperfect ILSs

The ILS is the Fourier transform of the weighting applied to the interferogram. This weighting consists of two parts: an artificially applied part to change the calculated spectrum and an unavoidable part which is due to the fact that the interferogram is finite in length (box car function), the divergence of the beam is non-zero (due to the non-zero entrance aperture), and several other effects which are due to misalignment (Davis et al., 2001, chapter 9). The ILS consisting of only the unavoidable parts of the line shape is called the ideal line shape.

The theoretical ideal ILS as defined in equation (3), when the instrument is well aligned, is a convolution of sinc and rectangular functions (defined in equations (1) and (2)), representing the finite length of the interferogram and the finite circular field of view (FOV) of the spectrometer (Davis et al., 2001).

$$SINC(\sigma, L) = 2L\frac{\sin(2\pi\sigma L)}{2\pi\sigma L} \tag{1}$$

$$RECT(\sigma, \sigma_0, \theta) = \begin{cases} \dfrac{2}{\sigma_0\theta^2} & if\ -0.5\sigma_0\theta^2 \le \sigma \le 0 \\ 0 & otherwise \end{cases} \tag{2}$$

$$ILS(\sigma, \sigma_0, L, \theta) = SINC(\sigma, L) * RECT(\sigma, \sigma_0, \theta) \tag{3}$$

where σ is the wavenumber, σ_0 is the central wavenumber, L is the optical path difference (OPD) and θ is the angular radius of the circular internal FOV of the spectrometer. For standard NDACC measuring conditions, $L \geq 180$ cm and θ defined by the entrance field stop size in the light path.

The LINEFIT software calculates the deviation of the measured ILS from the ideal ILS (Hase et al., 2001 and 2012). It retrieves a complex ME as a function of OPD, which is represented by a ME amplitude and a phase error (PE) (Hase et al., 1999). The ME amplitude is connected to the width of the ILS while the PE quantifies the degree of ILS asymmetry. For a perfectly aligned spectrometer, it would meet the

Atmos. Meas. Tech. Discuss., https://doi.org/10.5194/amt-2017-382
Manuscript under review for journal Atmos. Meas. Tech.
Discussion started: 10 January 2018

Atmospheric Measurement Techniques Discussions

ideal nominal ILS characteristics if smear and vignetting effects were neglected, and thus have an ME amplitude of unity and a PE of zero along the whole interferogram. However, if a FTIR spectrometer is subject to misalignment, the ME amplitude would deviate from unity and the PE deviate from zero (Hase et al., 2012). This results in an imperfect ILS.

3 Simulation of ILS degradation

We use the program ALIGN60 to simulate ILS degradation in a high resolution FTIR spectrometer typically used in the NDACC network. As a part of LINEFIT, ALIGN60 is a package for simulation of the ILS of misaligned cube-corner interferometers. It generates trustworthy results with respect to all types of misalignment (Hase et al., 1999). In this simulation, the entrance beam section was assumed to be circular with a diameter of 8.0 cm. The ILS was only calculated from positive side of interferogram. The smear and vignetting effects were not taken into account. The misalignment of a FTIR spectrometer can be expressed via two perpendicular axes perpendicular to the beam direction. For a circular entrance beam, the same misalignment in either direction results in a similar ILS. Thus, this work only considers misalignment in one axis.

The misalignments as inputs of ALIGN60 are listed in Table 1 and the resulting ILSs are shown in Fig. 1. All types of misalignment cause nonlinear ME deviations except decentering of measuring laser (*c*) and the constant shear (*d*) which mainly affect PE and result in linear PE deviation. Two types of ILS degradation are evident, one is referred to as positive ME and has a ME amplitude of larger than unity. The other one is referred to as negative ME and has a ME amplitude of less than unity. Typically, the increasing misalignment (*b*, *f*, *h* or *i*) causes negative ME amplitude and the decreasing misalignment (*e*, *g* or *j*) causes positive ME amplitude. For the same misalignment amplitude, the decreasing misalignment causes more ME deviation than the increasing misalignment. Regardless of positive or negative ME, the ME deviation shape depends on misalignment type and the same misalignment amplitude causes the same deviation in ME amplitude. The decentering of the entrance filed stop is

Atmos. Meas. Tech. Discuss., https://doi.org/10.5194/amt-2017-382
Manuscript under review for journal Atmos. Meas. Tech.
Discussion started: 10 January 2018

Atmospheric Measurement Techniques Discussions

equivalent to the linear increasing misalignment.

4 NDACC gases retrieval

4.1 Retrieval strategy

The influence of ILS degradation on all current NDACC gases, i.e., O_3, HNO_3, HCl, HF, $ClONO_2$, CH_4, CO, N_2O, C_2H_6, and HCN, is investigated here. Typical atmospheric vertical profiles of these gases are shown in Fig.2. There are five stratospheric gases and five tropospheric gases. The retrieval settings as recommended by the NDACC for all these gases are listed in Table 2. The latest version of profile retrieval algorithm SFIT4 v 0.9.4.4 is used (http://www.ndacc.org/). The basic principle of SFIT4 is using an optimal estimation technique for fitting calculated-to-observed spectra (Rodgers, 2000; Hannigan and Coffey, 2009). All spectroscopic line parameters are adopted from HITRAN 2008 (Rothman et al., 2009) in this study. This might not be ideal, but we keep it to achieve consistent results. A priori profiles of pressure, temperature and water vapor for the measurement days are interpolated from the National Centers for Environmental Protection and National Center for Atmospheric Research (NCEP/NCAR) reanalysis (Kalnay et al., 1996). A priori profiles of the target gases and the interfering gases except H_2O use the WACCM4 (Whole Atmosphere Community Climate Model) model data. We follow the NDACC standard convention with respect to micro windows (MWs) selection and the interfering gases consideration (https://www2.acom.ucar.edu/irwg/links). No de-weighting signal to noise ratios (SNR) are used except for CO and HCl which utilize a de-weighting SNR of 500 and 300, respectively.

The selection of the regularization (a priori covariance matrix $\mathbf{S}_a$ and SNR) cannot be easily standardised because it depends on the real variability for each gas. In optimal estimation, the selection of $\mathbf{S}_a$ is very important in the inversion process and, together with the measurement noise error covariance matrix $\mathbf{S}_\varepsilon$, will lead to the following averaging kernel matrix $\mathbf{A}$ (Rodgers, 2000):

$$\mathbf{A} = \mathbf{G}_y\mathbf{K}_x = (\mathbf{K}_x^T\mathbf{S}_\varepsilon^{-1}\mathbf{K}_x^T + \mathbf{S}_a^{-1})^{-1}\mathbf{K}_x^T\mathbf{S}_\varepsilon^{-1}\mathbf{K}_x \quad (4)$$

where $\mathbf{G}_y$ is the sensitivity of the retrieval to the measurement. $\mathbf{K}_x$ is weighting function matrix or Jacobian matrix that links the measurement vector $\boldsymbol{y}$ to the state vector $\boldsymbol{x}$: $\Delta\boldsymbol{y}=\mathbf{K}_x\Delta\boldsymbol{x}$. $\mathbf{A}$ characterizes the vertical information contained in the FTIR retrievals. In this study, we assume $\mathbf{S}_\varepsilon$ to be diagonal and its diagonal elements are the

Atmos. Meas. Tech. Discuss., https://doi.org/10.5194/amt-2017-382
Manuscript under review for journal Atmos. Meas. Tech.
Discussion started: 10 January 2018

Atmospheric Measurement Techniques Discussions

inverse square of the SNR. The vertical information content of the retrieved target gas profile can be quantified by the number of degrees of freedom for signal (DOFs), which is the trace of **A**, defined in Rodgers (2000) by:

$$d_s = tr(\mathbf{A}) = tr((\mathbf{K}_x^T\mathbf{S}_\varepsilon^{-1}\mathbf{K}_x^T + \mathbf{S}_a^{-1})^{-1}\mathbf{K}_x^T\mathbf{S}_\varepsilon^{-1}\mathbf{K}_x^T) \quad (5)$$

The diagonal elements of $\mathbf{S}_a$ represent the assumed variability of the target gas volume mixing ratio (VMR) at a given altitude, and the off diagonal elements represent the correlation between the VMR at different altitudes. We can see in Table 3 that, except CO and HCN, the target gases are using an a priori covariance matrix with diagonal elements constant with altitude corresponding to 10, 20, 50 or 100 % variability; the largest variabilities are for HNO_3, HCl and $ClONO_2$. For CO, the diagonal elements of $\mathbf{S}_a$ correspond to 27% from ground to 34 km and decrease down to 11% at the top of atmosphere. For HCN, the diagonal elements of $\mathbf{S}_a$ correspond to 79% from ground to 5 km and decrease down to 21% at the top of atmosphere. No correlation of off diagonal matrix elements is used in all retrievals except for $ClONO_2$ which uses exponential correlation with a HWHM (half with at half-maximum) of 8 km. The SNR values for all retrievals are the real values taken from each individual spectrum. The ILSs for all retrievals are using the simulations in section 3.

4.2 Averaging kernels

Beside the a priori covariance matrix $\mathbf{S}_a$ and $\mathbf{S}_\varepsilon$, the averaging kernel matrix **A** also depends on retrieval parameters including solar zenith angle (SZA), the spectral resolution, and the choice of spectral micro windows (MW). The rows of **A** are the so called averaging kernels and they represent the sensitivity of the retrieved profile to the real profile. Their FWHM is a measure of the vertical resolution of the retrieval at a given altitude. The area of averaging kernels represents sensitivity of the retrievals to the measurement. This sensitivity at altitude k is calculated as the sum of the elements of the corresponding averaging kernels, $\sum_i \mathbf{A}_{ki}$. It indicates the fraction of the retrieval at each altitude that comes from the measurement rather than from the a priori information (Rodgers, 2000). A value close to zero at a certain altitude indicates that the retrieved profile at that altitude is nearly independent of measurement and is therefore approaching the a priori profile.

The averaging kernel matrices of these ten NDACC gases are shown in Fig. 3. Fig. 4 is the corresponding averaging kernels and their areas. The altitude ranges with

Atmos. Meas. Tech. Discuss., https://doi.org/10.5194/amt-2017-382
Manuscript under review for journal Atmos. Meas. Tech.
Discussion started: 10 January 2018

Atmospheric Measurement Techniques Discussions

sensitivity larger than 0.5 and the corresponding DOFs are summarized in Table 3. These sensitive ranges indicate that the retrieved profile information comes by more than 50% from measurement, or, in other words, that the a priori information influences the retrieval by less than 50%. Each gas has different sensitive range. The sensitive range for HCN, CO and C_2H_6 is mainly tropospheric, and for $ClONO_2$, HCl and HF is mainly stratospheric. O_3, CH_4 and N_2O have high retrieval sensitivity in both troposphere and stratosphere. The HNO_3 has high retrieval sensitivity in stratosphere and in atmospheric boundary layer below 1.5 km.

4.3 Error analysis

As listed in Table 2, we classified errors as systematic or random according to whether they are constant between consecutive measurements, or vary randomly. For comparison, the error items considered in error analysis are the same for the retrieval of all gases. The smoothing error $\mathbf{E}_s$ is calculated via equation (6), the measurement error $\mathbf{E}_m$ is calculated via equation (7), and all other error items $\mathbf{E}_{var}$ are calculated via equation (8) (Rodgers, 2000).

$$\mathbf{E}_s = (\mathbf{A} - \mathbf{I})\mathbf{S}_a(\mathbf{A} - \mathbf{I})^T \quad (6)$$

$$\mathbf{E}_m = \mathbf{G}_y\mathbf{S}_\varepsilon\mathbf{G}_y^T \quad (7)$$

$$\mathbf{E}_{\mathrm{var}} = \mathbf{G}_y\mathbf{K}_{\mathrm{var}}\mathbf{S}_{\mathrm{var}}\mathbf{K}_{\mathrm{var}}^T\mathbf{G}_y^T \quad (8)$$

where $\mathbf{S}_{var}$ is the error covariance matrix of *var*. $\mathbf{K}_{var}$ is weighting function matrix of *var*. Here *var* refers to one of the error items in Table 2 except smoothing error and measurement error. In this study, the a priori error covariances for all non-retrieval parameters are set the same for all gases retrieval.

Figs.5 and 6 show the error components contributing to the systematic error and random error covariance matrices of all NDACC gases, as well as the combined errors. The structure in the error profiles shape reflects the effect of the propagation of different errors in the retrieval process. The dominant sources of systematic errors and random errors for all gases are listed in Table 4. For most gases, the dominant sources of systematic errors are smoothing error, line intensity error and line pressure broadening error. The dominant sources of random errors are measurement error and zero level.

5 ILS influence study

Atmos. Meas. Tech. Discuss., https://doi.org/10.5194/amt-2017-382
Manuscript under review for journal Atmos. Meas. Tech.
Discussion started: 10 January 2018

Atmospheric Measurement Techniques Discussions

This section presents the ILS influence study, whereby the degraded ILSs that simulated by ALIGN60 are used in the SFIT forward model, and the fractional difference (D%) in various quantities for each gas relative to the retrieval with an ideal ILS are computed. For each gas, this section only selects one typical spectrum for study. The consistency of the resulting deduction will be evaluated in section 6. All spectra were recorded on a clear day at Hefei on February 16, 2017. For all spectra used in this study, the actual ILS degradation of the FTIR spectrometer is less than 1.3% and can be regarded as ideal. We have taken the retrievals with an ideal ILS as the reference. The fractional difference is defined here as,

$$\mathbf{D}\% = \frac{\mathbf{X} - \mathbf{X}_{ref}}{\mathbf{X}_{ref}} \times 100 \quad (11)$$

where **X** is a vector which can include multiple elements such as gas profile or only one element such as DOFs, root mean square of fitting residual (RMS), total column, total random uncertainty, total systematic uncertainty, or total uncertainty. The total random uncertainty and systematic uncertainty are the sum in quadrature of each individual uncertainty listed in Table 2, and the total uncertainty is the sum in quadrature of total random uncertainty and total systematic uncertainty. $\mathbf{X}_{ref}$ is the same as **X** but for the nominal ideal ILS. For all gases, the retrievals with all levels of ILS degradation fulfill the following filter criteria:

1) The RMSs of the residual (difference between measured and calculated spectra after the fit) in all fitting windows has to be less than 3%.

2) The retrievals should converge for all levels of ILS degradation.

3) The concentrations of the target and interfering gases at each sub layer should be positive.

4) The solar intensity variation (SIV) should be less than 10%. The SIV within the duration of a spectrum is the ratio of the standard deviation to the average of the measured solar intensities.

5.1 ME amplitude and PE influence

In order to determine how the ILS degradation affects the NDACC gas retrievals,

Atmos. Meas. Tech. Discuss., https://doi.org/10.5194/amt-2017-382
Manuscript under review for journal Atmos. Meas. Tech.
Discussion started: 10 January 2018

the results deduced from ILS considering both ME amplitude and PE are compared to those only considering ME amplitude or PE. All types of ILS degradation in section 3 are used in this study. Fig.7 exemplifies the case of ILS *j*, where the differences in total column, RMS, random uncertainty, systematic uncertainty, total uncertainty, and DOFs for each gas relative to the retrieval with an ideal ILS are compared. Fig.8 shows the fractional difference in profile of each gas for ILS *j*. The results show that the influence of ILS degradation on the total column, RMS, random uncertainty, systematic uncertainty, total uncertainty, DOFs, and profile can be approximated by the linear sum of individual ME amplitude influence and PE influence. The PE influence is of secondary importance compared with the ME amplitude influence. The comparisons for the results retrieved with ILS *a* to *i* come to the same conclusions.

Figs.9 and 10 show the influence of ILS *a* to *j* on total column and profile of all NDACC gases. The resulting influence amounts depend on deviation amount and deviation shape of ME. For positive MEs, in most cases, the ILS *j* causes the maximum influence, and for negative MEs, the ILS *i* causes the maximum influence. In a real instrument, the misalignment is a combination of misalignment *a* to *j*. In principle, it should not cause influence exceeding misalignment *i* or *j* for the same misalignment amplitude. In the following, misalignment *i* and *j* are selected on behalf of negative and positive ME respectively to investigate how the ILS degradation influence the NDACC gas retrievals.

5.2 Sensitivity study

We simulated seven levels of negative ME *i* and positive ME *j* with ALIGN60, and incorporated them in the SFIT forward model, and then calculated the fractional difference in various quantities for each gas relative to the retrieval with an ideal ILS. The misalignments as inputs of ALIGN60 and the resulting ILSs are shown in Figs. 11 and 13. The corresponding Haidinger fringes at the maximum misalignment position are shown in Figs. 12 and 14. The ME deviation, decenter of Haidinger fringes and ILS deterioration varying over misalignment are evident. Fig.15 is the sensitivity of total column with respect to different levels of ILS degradation. Figs. 16

Atmos. Meas. Tech. Discuss., https://doi.org/10.5194/amt-2017-382
Manuscript under review for journal Atmos. Meas. Tech.
Discussion started: 10 January 2018

297 ~ 19 are the same as Fig. 15 but for DOFs, RMS, uncertainty and profile. The results
298 show that the ILS degradation affected total column, RMS, DOFs, retrieval
299 uncertainty, and profile. Generally, the larger the ME deviation, the larger the
300 influence. The positive and negative ME have opposite influence on total column,
301 DOFs, total uncertainty and profile.

302 With respect to total column, the influence of ILS degradation on stratospheric
303 gases is larger than the tropospheric gases. For O_3 and HNO_3, positive ME causes an
304 overestimated total column and negative ME causes an underestimated total column.
305 For other gases, negative ME causes an overestimated total column and positive ME
306 causes an underestimated total column. For all gases except O_3 and CH_4, the positive
307 ME influence is larger than the negative ME influence. For O_3 and CH_4, the negative
308 ME influence is larger than the positive ME influence.

309 For all gases, positive ME increases the DOFs and negative ME decreases DOFs.
310 For all gases except HF and CH_4, both positive ME and negative ME increase RMS.
311 For HF, positive ME increases RMS while negative ME decreases RMS. For CH_4,
312 positive ME decreases RMS and negative ME increases RMS.

313 The influence on systematic uncertainty and random uncertainty depends on ME
314 deviation type and gas type. The influence on total uncertainty is the combination of
315 the influence on total systematic uncertainty and total random uncertainty. For all
316 gases except O_3, positive ME decreases total uncertainty and negative ME increases
317 total uncertainty. For O_3, positive ME increases total uncertainty and negative ME
318 decreases total uncertainty.

319 The ILS degradation causes an evident difference in profile within the altitude
320 ranges that show high retrieval sensitivity in Fig.4. Positive ME has more influence on
321 tropospheric gas than negative ME. Whereas, negative ME has more influence on
322 stratospheric gas than positive ME.

323 ## 5.3 Discussion and analysis

324 For each gas, the *a priori* covariance matrices of $\mathbf{S}_a$, $\mathbf{S}_\varepsilon$, and $\mathbf{S}_{var}$ are the same in
325 the aforementioned study. According to equations 6 ~ 8, we conclude that the ILS

Atmos. Meas. Tech. Discuss., https://doi.org/10.5194/amt-2017-382
Manuscript under review for journal Atmos. Meas. Tech.
Discussion started: 10 January 2018

degradation altered the weighting function matrix $\mathbf{K}_x$ and eventually altered the quantities such as the total column, RMS, random uncertainty, systematic uncertainty, total uncertainty, DOFs, and profile. The change of $\mathbf{K}_x$ is attributed to the fact that the ILS degradation alters gas absorption line shape and hence alters the structure of calculated spectra, and aggravates the mismatch between the calculated spectra and the measured spectra.

The stratospheric gases are more sensitive to ILS degradation than the tropospheric gases, and the $ClONO_2$ exhibits the largest sensitivity. This is because the absorption structure in stratosphere is narrower than that in troposphere, and is more easily affected by ILS degradation. We set the acceptable fractional difference in total column for $ClONO_2$ and other NDACC gases as 10% and 1%, respectively. Considering the excessively large of 28% ME deviation seldom occurred within NDACC network because of the regular alignment at each site, the permitted maximum ILS degradation for each gas is deduced in Table 5.

6 Consistency evaluation

For each gas, section 5 only selects one spectrum for study. This section uses all spectra recorded at Hefei from September 2014 to April 2017 to evaluate the consistency of above study. These spectra span a large difference in atmospheric water vapor, SZAs, surface pressures, surface temperatures, wind speeds, and wind directions (Fig. 20). All retrievals fulfill the above filter criteria are included in this study. A simulated ILS *j* with maximum ME amplitude deviation of 5% is used in the retrieval. The results are compared to the retrievals deduced from an ideal ILS. The Hefei site has run NDACC observations with the Bruker 125HR FTS for more than two years. We regularly use a low-pressure HBr cell to diagnose the misalignment of the spectrometer and to realign the instrument when indicated. For all spectra used in this study, the ILS can be regarded as ideal and thus the retrievals with ideal ILS can be taken as the reference.

Figs. 21 ~ 26 present the fractional difference in total column, RMS, total uncertainty, and DOFs under different humidity, pressure, SZA, temperature, wind

Atmos. Meas. Tech. Discuss., https://doi.org/10.5194/amt-2017-382
Manuscript under review for journal Atmos. Meas. Tech.
Discussion started: 10 January 2018

direction, and wind speed. The results show that the fractional difference in total column and total uncertainty for all gases are consistent under different meteorological conditions and SZAs. The fractional difference in DOFs for all gases except N_2O and HCN are also consistent. For N_2O and HCN, the variation of fractional difference in DOFs is larger than that of total column and total uncertainty. But most of them are less than 10% and independent of meteorological conditions and SZAs. For most gases, the fractional difference in RMS exhibits more scatters than the total column, total uncertainty, and DOFs. However, they are also independent of meteorological conditions and SZAs, and most of them are less than 10%. In general, the influence of ILS degradation on NDACC gases retrieval shows good consistency under different meteorological conditions and SZAs.

6 Conclusion

We assessed the influence of instrumental line shape degradation on all current NDACC gases retrieval via investigation of sensitivities of total column, root mean square of fitting residual, total random uncertainty, total systematic uncertainty, total uncertainty, degrees of freedom, and profile with respect to modulation efficiency deviations. The study concluded that the influence of instrumental line shape degradation can be approximated by the linear sum of individual modulation efficiency amplitude influence and phase error influence. The phase error influence is of secondary importance compared with the modulation efficiency amplitude influence. The influence amounts depend on deviation amount and deviation shape of the modulation efficiency.

For total column retrieval, the stratospheric gases are more sensitive to instrumental line shape degradation than the tropospheric gases. For profile retrieval, the positive modulation efficiency has more influence on tropospheric gases than the stratospheric gases. While the negative modulation efficiency has more influence on stratospheric gases than the tropospheric gases. The influence of instrumental line shape degradation on NDACC gas retrievals shows good consistency under different meteorological conditions and solar zenith angle. Finally, as summarized in Table 5,

384 we deduced maximum instrumental line shape deviations allowable for suppressing
385 the influence within a specified acceptable ranges.

386 ## 7 Acknowledgements

387 This work is jointly supported by the National High Technology Research and
388 Development Program of China (No. 2016YFC0200800, 2016YFC0203302), the
389 National Science Foundation of China (No. 41605018, No. 41405134, No.41775025,
390 No. 41575021, No. 51778596, No. 91544212, No. 41722501), Anhui Province
391 Natural Science Foundation of China (No. 1608085MD79), and the German Federal
392 Ministry of Education and Research (BMBF) (Grant No. 01LG1214A). The
393 processing environment of SFIT4 and some plot programs are provided by National
394 Center for Atmospheric Research (NCAR), Boulder, Colorado, USA. The NDACC
395 networks are acknowledged for supplying the SFIT software and advice.

396 ## 8 References

397 Davis, S. P., Abrams, M. C., and Brault, J. W.: Fourier transform spectrometry,
398 Academic Press, ISBN: 0-12-042510-6, 2001.

399 Duchatelet P., Demoulin P., Hase F., Ruhnke R., Feng W., Chipperfield M. P., Bernath
400 P. F., Boone C. D., Walker K. A., and Mahieu E.: Hydrogen fluoride total and
401 partial column time series above the Jungfraujoch from long term FTIR
402 measurements: Impact of the line shape model, characterization of the error
403 budget and seasonal cycle, and comparison with satellite and model data, J.
404 Geophys. Res., 115, D22306, doi:10.1029/2010JD014677, 2010.

405 Feist D. G., Arnold S. G., Hase F., and Ponge D.: Rugged optical mirrors for Fourier
406 transform spectrometers operated in harsh environments, Atmos. Meas. Tech., 9,
407 2381–2391, www.atmos-meas-tech.net/9/2381/2016/ doi:10.5194/amt
408 -9-2381-2016, 2016.

409 Hannigan, J. and Coffey, M.: semiautonomous FTS observation system for remote
410 sensing of stratospheric and tropospheric gases, Journal of Atmospheric and
411 Oceanic Technology . 09/2009; 26(9). DOI: 10.1175/2009JTECHA1230.1

412 Hase, F., Demoulin, P., Sauval, A., Toon, G. C., Bernath, P., Goldman, A., Hannigan, J.,

413 Rinsland C.: An empirical line-by-line model for the infrared solar
414 transmittance spectrum from 700 to 5000 cm^{-1}, J. Quant. Spectrosc. Radiat.
415 Transfer, 2006, 102, 450 - 463.
416 Hase, F.: Improved instrumental line shape monitoring for the ground-based,
417 high-resolution FTIR spectrometers of the Network for the Detection of
418 Atmospheric Composition Change, Atmos. Meas. Tech., 5, 603–610,
419 doi:10.5194/amt-5-603-2012,2012.
420 Hase, F., Drouin, B. J., Roehl, C. M., Toon, G. C., Wennberg, P. O., Wunch, D.,
421 Blumenstock, T., Desmet, F., Feist, D. G., Heikkinen, P., De Mazière, M.,
422 Rettinger, M., Robinson, J., Schneider, M., Sherlock, V., Sussmann, R., Té, Y.,
423 Warneke, T., and Weinzierl, C.: Calibration of sealed HCl cells used for TCCON
424 instrumental line shape monitoring, Atmos. Meas. Tech., 6, 3527-3537,
425 doi:10.5194/amt-6-3527-2013, 2013.
426 Hase, F., Blumenstock, T., and Paton-Walsh, C.: Analysis of the instrumental line
427 shape of high-resolution Fourier transform IR spectrometers with gas cell
428 measurements and new retrieval software, Appl. Optics, 38, 3417–3422, 1999.
429 Kalnay E., Kanamitsu M., Kistler R., et al. (1996) The NCEP/NCAR 40-year
430 reanalysis project. Bulletin of the American Meteorological Society, 77, 437-472.
431 Kurylo, M. J.: Network for the detection of stratospheric change (NDSC), SPIE
432 Proceedings 1991, P. Soc. Photo-Opt. Ins., 1491, 168–174, 1991.
433 Kohlhepp, R., Barthlott, S., Blumenstock, T., Hase, H., Kaiser, I., Raffalski, U., and
434 Ruhnke, R.: Trends of HCl, $ClONO_2$, and HF column abundances from
435 ground-based FTIR measurements in Kiruna (Sweden) in comparison with
436 KASIMA model calculations, Atmos. Chem. Phys., 11, 4669–4677, 2011
437 www.atmos-chem-phys.net/11/4669/2011/doi:10.5194/acp-11-4669-2011
438 Messerschmidt, J., Macatangay, R., Notholt, J., Petri, C., Warneke, T., and Weinzierl,
439 C.: Side by side measurements of CO_2 by ground-based Fourier transform
440 spectrometry (FTS), Tellus B, 62, 749–758, oi:10.1111/j.1600-0889.2010.00491.x
441 ,2010.
442 Olsen, S. C. and Randerson, J. T.: Differences between surface and column

443 atmospheric CO_2 and implications for carbon cycle research, J. Geophys.
444 Res.-Atmos., 109, D02301, doi:10.1029/2003JD003968, 2004.
445 Schneider, M., Redondas, A., Hase, F., Guirado, C., Blumenstock, T., and Cuevas, E.:
446 Comparison of ground-based Brewer and FTIR total column O_3 monitoring
447 techniques, Atmos. Chem. Phys., 8, 5535–5550, doi:10.5194/acp-8-5535-2008,
448 2008.
449 Rodgers, C. D.: Inverse methods for atmospheric sounding: Theory and Practice,
450 Series on Atmospheric, Oceanic and Planetary Physics, Vol. 2, World Scientific
451 Publishing Co., Singapore, 2000.
452 Rothman, L. S., Gordon, I. E., Barbe, A., Benner, D. C., Bernath, P. F., Birk, M.,
453 Boudon, V., Brown, L. R., Campargue, A., Champion, J.-P., Chance, K., Coudert,
454 L. H., Danaj, V., Devi, V. M., Fally, S., Flaud, J.-M., Gamache, R. R., Goldmanm,
455 A., Jacquemart, D., Kleiner, I., Lacome, N., Lafferty, W. J., Mandin, J.-Y., Massie,
456 S. T., Mikhailenko, S. N., Miller, C. E., Moazzen-Ahmadi, N., Naumenko, O. V.,
457 Nikitin, A. V., Orphal, J., Perevalov, V. I., Perrin, A., Predoi-Cross, A., Rinsland, C.
458 P., Rotger, M., Šime. cková, M., Smith, M. A. H., Sung, K., Tashkun, S. A.,
459 Tennyson, J., Toth, R. A., Vandaele, A. C., and Vander Auwera, J.: The Hitran
460 2008 molecular spectroscopic database, J. Quant. Spectrosc. Ra., 110, 533–572,
461 2009.
462 Vigouroux, C., De Mazi ère, M., Demoulin, P., Servais, C., Hase, F.,Blumenstock, T.,
463 Kramer, I., Schneider, M., Mellqvist, J., Strandberg, A., Velazco, V., Notholt, J.,
464 Sussmann, R., Stremme, W., Rockmann, A., Gardiner, T., Coleman, M., and
465 Woods, P.: Evaluation of tropospheric and stratospheric ozone trends over Western
466 Europe from ground-based FTIR network observations, Atmos. Chem. Phys., 8,
467 6865–6886, 2008, http://www.atmos-chem-phys.net/8/6865/2008/.
468 Vigouroux, C., Blumenstock, T., Coffey, M., Errera, Q., Garc á, O., Jones, N. B.,
469 Hannigan, J. W., Hase, F., Liley, B., Mahieu, E., Mellqvist, J., Notholt, J., Palm,
470 M., Persson, G., Schneider, M., Servais, C., Smale, D., Th ölix, L., and De Mazi ère,
471 M.: Trends of ozone total columns and vertical distribution from FTIR
472 observations at eight NDACC stations around the globe, Atmos. Chem. Phys., 15,

2915-2933, doi:10.5194/acp-15-2915-2015, 2015.

Washenfelder, R. A.: Column abundances of carbon dioxide and methane retrieved from ground-based near-infrared solar spectra, PhD thesis, California Institute of Technology, Pasadena, California (available at: http://thesis.library.caltech.edu), 2006.

Wunch, D., Toon, G. C., Wennberg, P. O., Wofsy, S. C., Stephens, B. B., Fischer, M. L., Uchino, O., Abshire, J. B., Bernath, P., Biraud, S. C., Blavier, J.-F. L., Boone, C., Bowman, K. P., Browell, E. V., Campos, T., Connor, B. J., Daube, B. C., Deutscher, N. M., Diao, M., Elkins, J. W., Gerbig, C., Gottlieb, E., Griffith, D. W. T., Hurst, D. F., Jiménez, R., Keppel-Aleks, G., Kort, E. A., Macatangay, R., Machida, T., Matsueda, H., Moore, F., Morino, I., Park, S., Robinson, J., Roehl, C. M., Sawa, Y., Sherlock, V., Sweeney, C., Tanaka, T., and Zondlo, M. A.: Calibration of the Total Carbon Column Observing Network using aircraft profile data, Atmos. Meas. Tech., 3, 1351–1362, doi:10.5194/amt-3-1351-2010, 2010.

Wunch, D., Toon, G. C., Blavier, J.-F. L.,Washenfelder, R., Notholt, J., Connor, B. J., Griffith, D. W. T., Sherlock, V., and Wennberg, P. O.: The Total Carbon Column Observing Network, Phil. T. Roy. Soc. A, 369, 2087–2112, doi:10.1098/rsta.2010.0240, 2011.

Wunch, D., Toon G. C., Sherlock V., Deutscher N. M., Liu C., Feist D. G., and Wennberg P. O.: The Total Carbon Column Observing Network's GGG2014 Data Version. 10.14291/tccon.ggg2014.documentation.R0/1221662, 2015.

Sun, Y., Palm, M., Weinzierl, C., Petri, C., Notholt, J., Wang, Y., and Liu, C.: Technical note: Sensitivity of instrumental line shape monitoring for the ground-based high-resolution FTIR spectrometer with respect to different optical attenuators, Atmos. Meas. Tech., 10, 989-997, doi: 10.5194/amt-10-989-2017, 2017.

9 Figs

Atmos. Meas. Tech. Discuss., https://doi.org/10.5194/amt-2017-382
Manuscript under review for journal Atmos. Meas. Tech.
Discussion started: 10 January 2018

Atmospheric Measurement Techniques Discussions

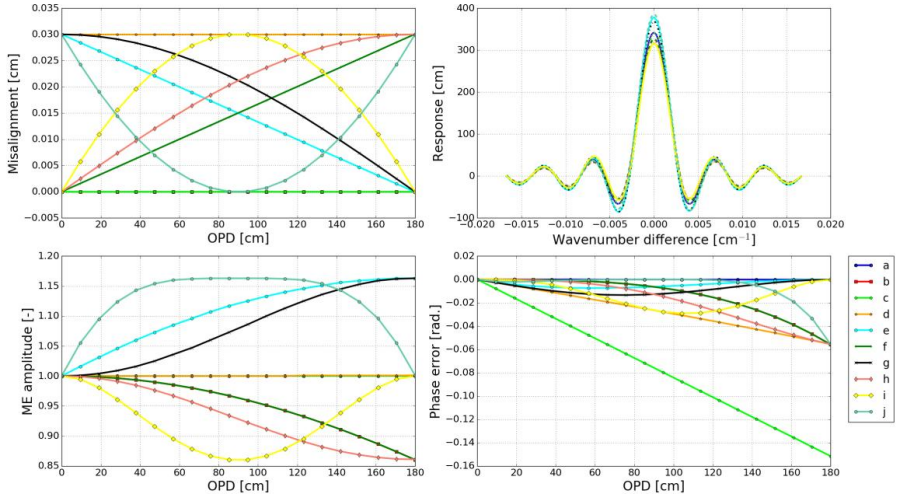

Fig.1. Simulated ILS degradation with respect to different types of misalignment. The results are derived from ALIGN60. Top left demonstrates different types of misalignment (*a* to *j*) used in the simulation, top right is the resulting ILS, bottom left is the resulting ME amplitude, and bottom right is the resulting PE. Descriptions for the misalignment *a* to *j* are listed in Table 1.

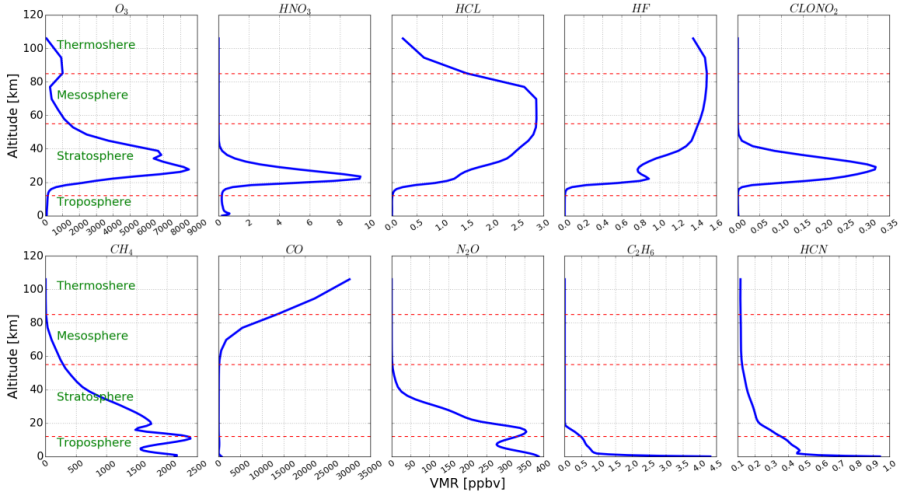

Fig.2. Typical profiles of ten NDACC gases. Bottom panels are five tropospheric gases, i.e., CH_4, CO, N_2O, C_2H_6, and HCN. Top panels are five stratospheric gases, i.e., O_3, HNO_3, HCl, HF, and $ClONO_2$. Although the CO concentration above 60 km is much higher than that in the troposphere, it is regarded as tropospheric gas because it is an anthropologic pollution gas and shows large variation in troposphere.

Atmos. Meas. Tech. Discuss., https://doi.org/10.5194/amt-2017-382
Manuscript under review for journal Atmos. Meas. Tech.
Discussion started: 10 January 2018

Atmospheric Measurement Techniques Discussions

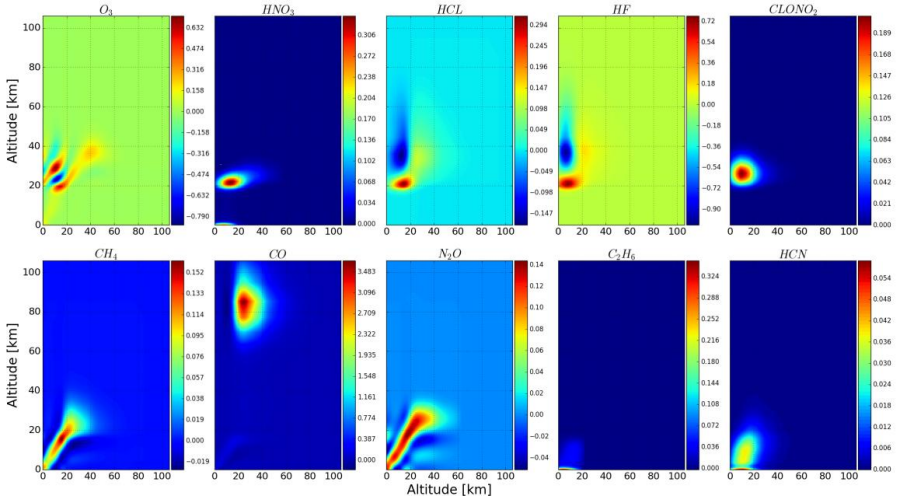

512
513 Fig.3. Averaging kernel matrices of ten NDACC gases. The deeper the color, the higher the
514 retrieval sensitivity. They are deduced from the spectra recorded at Hefei on September 8, 2015
515 with an ideal ILS.

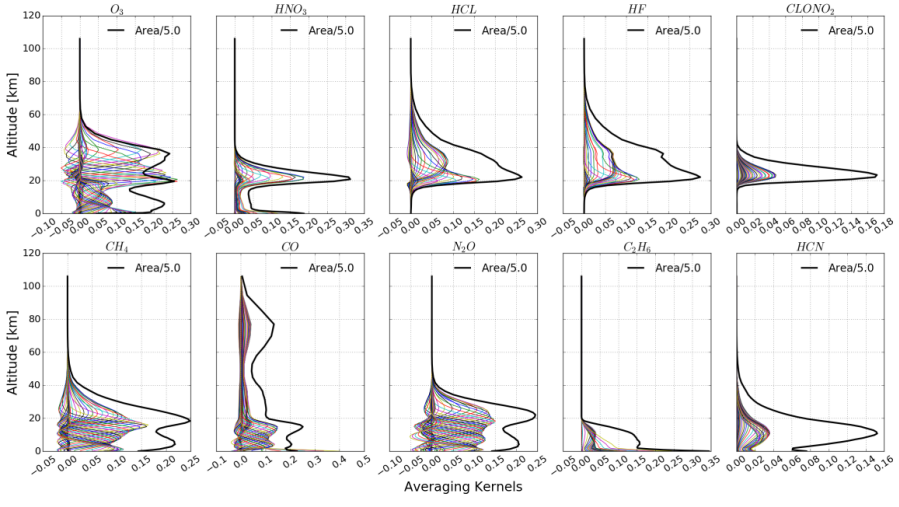

516
517 Fig.4 Averaging kernels of ten NDACC gases (color fine lines), and their area scaled by a factor of
518 0.2 (black bold line).

Atmos. Meas. Tech. Discuss., https://doi.org/10.5194/amt-2017-382
Manuscript under review for journal Atmos. Meas. Tech.
Discussion started: 10 January 2018

Atmospheric Measurement Techniques Discussions

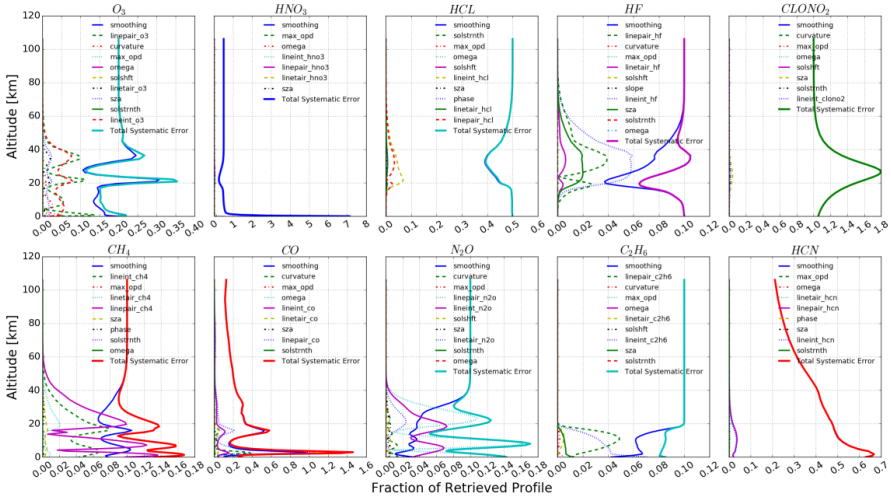

519

520 Fig.5. Ground-based FTIR systematic errors for ten NDACC gases retrieval. They are deduced
521 from the spectra used in section 5 with an ideal ILS.

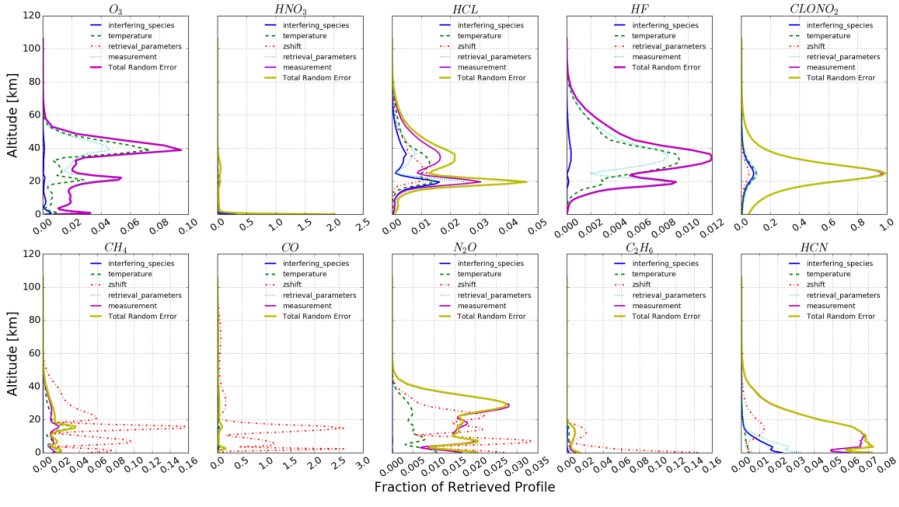

522

523 Fig.6. The same as Fig.5 but for random errors.

Atmos. Meas. Tech. Discuss., https://doi.org/10.5194/amt-2017-382
Manuscript under review for journal Atmos. Meas. Tech.
Discussion started: 10 January 2018

Atmospheric Measurement Techniques Discussions

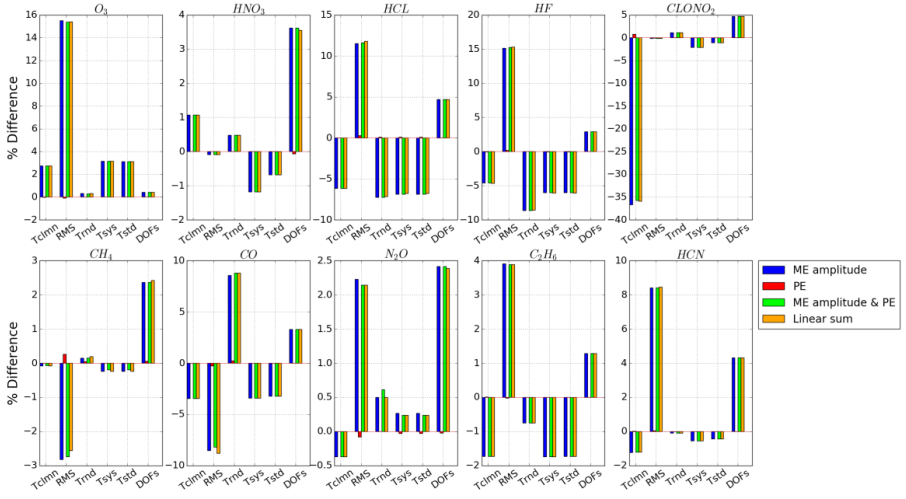

Fig.7. Fractional difference in total column, RMS, total random uncertainty, total systematic uncertainty, total uncertainty, and DOFs for misalignment *j*. "ME amplitude" represents the ILS only taken ME amplitude deviation into account. "PE" represents the ILS only taken PE deviation into account. "ME amplitude & PE" represents the ILS taken both ME amplitude and PE deviations into account. "Linear sum" represents the fractional difference of each item is linear sum of "ME amplitude" and "PE". The ME amplitude and PE are obtained from ALIGN60 with misalignment *j* in Fig.1.

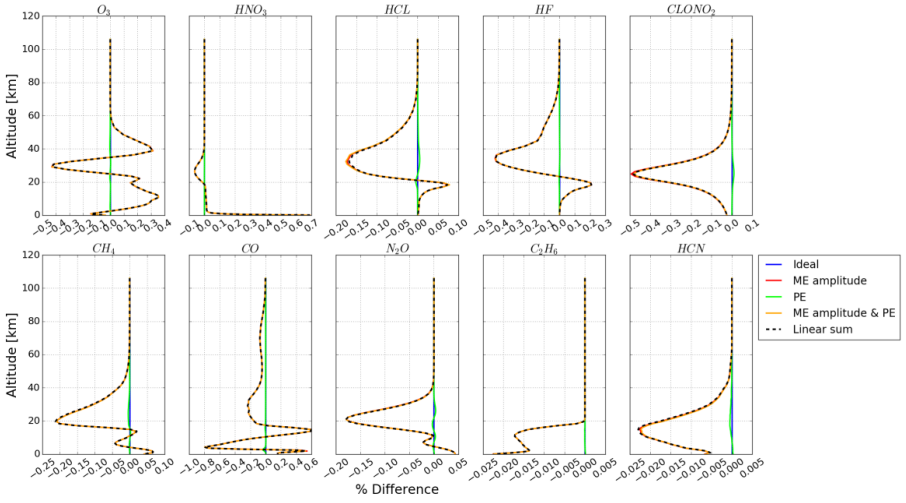

Fig.8. Fractional difference in profile for misalignment *j*. "ME amplitude" represents the ILS only taken ME amplitude deviation into account. "PE" represents the ILS only taken PE deviation into account. "ME amplitude & PE" represents the ILS taken both ME amplitude and PE deviations into account. "Linear sum" represents the fractional difference of each item is linear sum of "ME amplitude" and "PE". The ME amplitude and PE are obtained from ALIGN60 with misalignment *j* in Fig.1.

Atmos. Meas. Tech. Discuss., https://doi.org/10.5194/amt-2017-382
Manuscript under review for journal Atmos. Meas. Tech.
Discussion started: 10 January 2018

Atmospheric Measurement Techniques Discussions

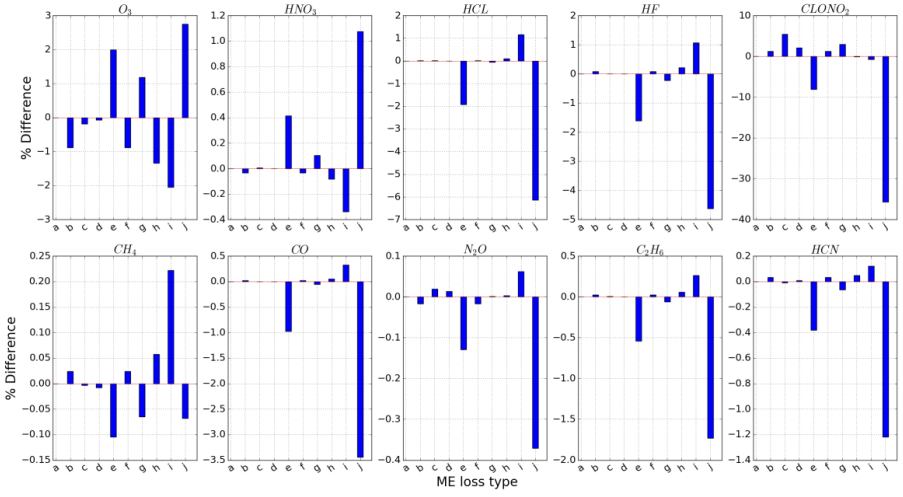

539

540 Fig.9. Sensitivity of total column to different types of ILS degradation. The ILS *a* to *j* correspond
541 to misalignment *a* to *j* in Table1.

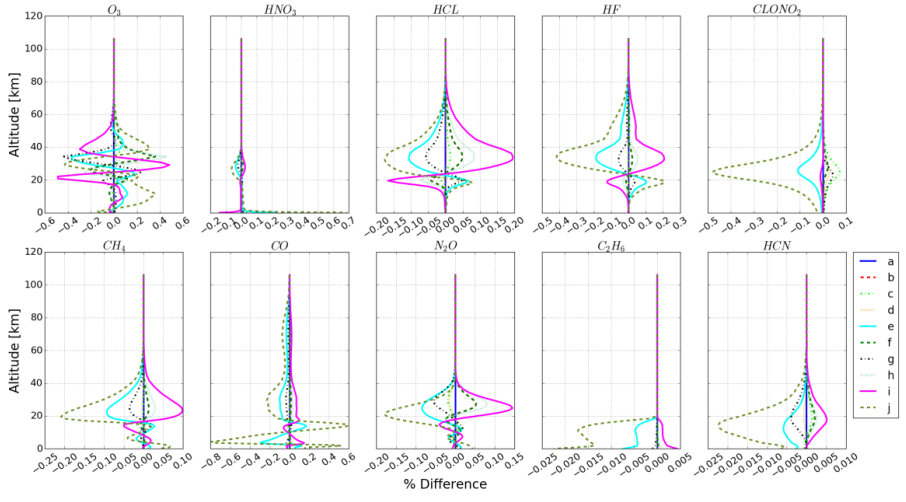

542

543 Fig.10. Sensitivity of profile to different types of ILS degradation. The ILS *a* to *j* correspond to
544 misalignment *a* to *j* in Table1.

Atmos. Meas. Tech. Discuss., https://doi.org/10.5194/amt-2017-382
Manuscript under review for journal Atmos. Meas. Tech.
Discussion started: 10 January 2018

Atmospheric Measurement Techniques Discussions

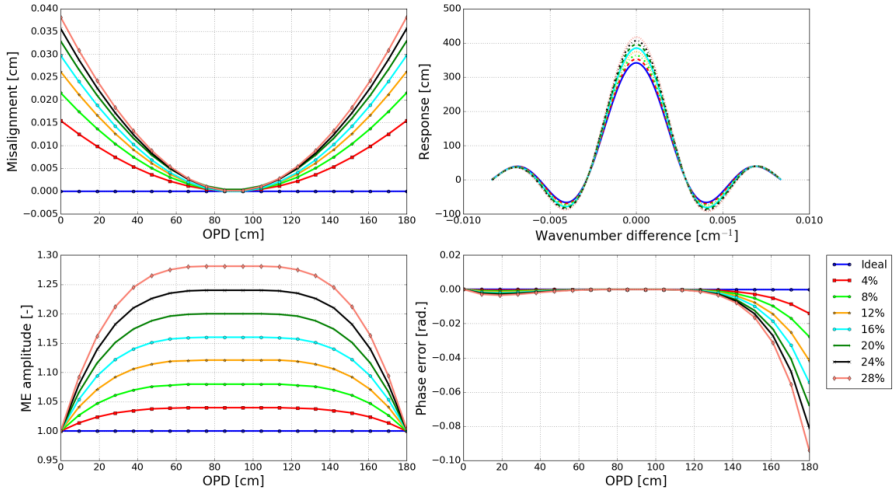

545

546 Fig.11. Simulated positive ME deviations along with OPD. Top left demonstrates the
547 misalignment, top right is the resulting ILS, bottom left is the resulting ME amplitude, and bottom
548 right is the resulting PE.

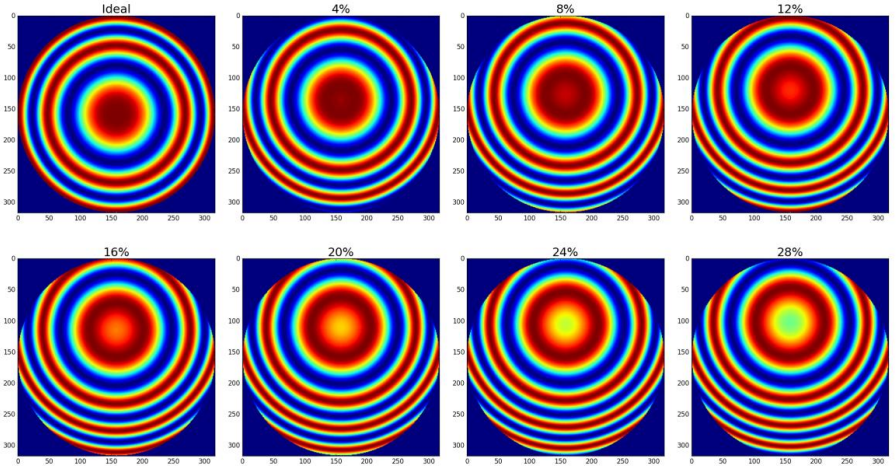

549

550 Fig.12. The Haidinger fringes at maximum OPD (the maximum misalignment position) for Fig. 11

Atmos. Meas. Tech. Discuss., https://doi.org/10.5194/amt-2017-382
Manuscript under review for journal Atmos. Meas. Tech.
Discussion started: 10 January 2018

Atmospheric Measurement Techniques Discussions

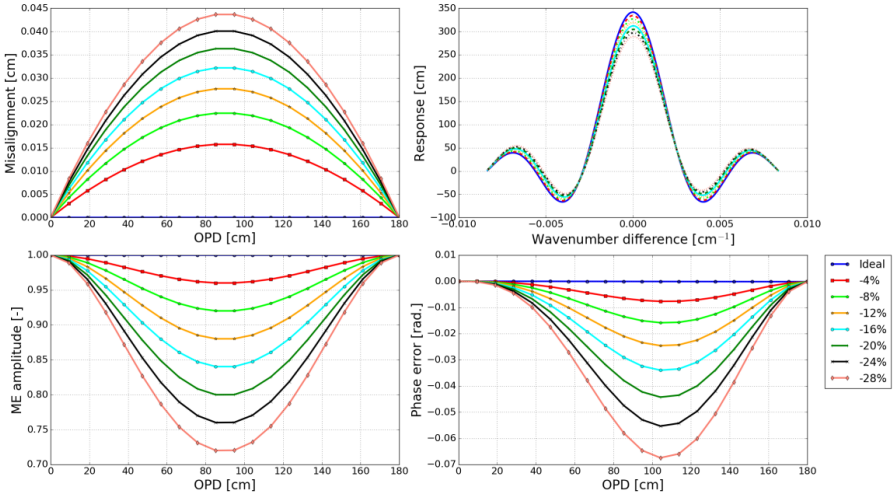

551
552 Fig.13. Simulated negative ME deviations along with OPD. Top left demonstrates the
553 misalignment, top right is the resulting ILS, bottom left is the resulting ME amplitude, and bottom
554 right is the resulting PE.

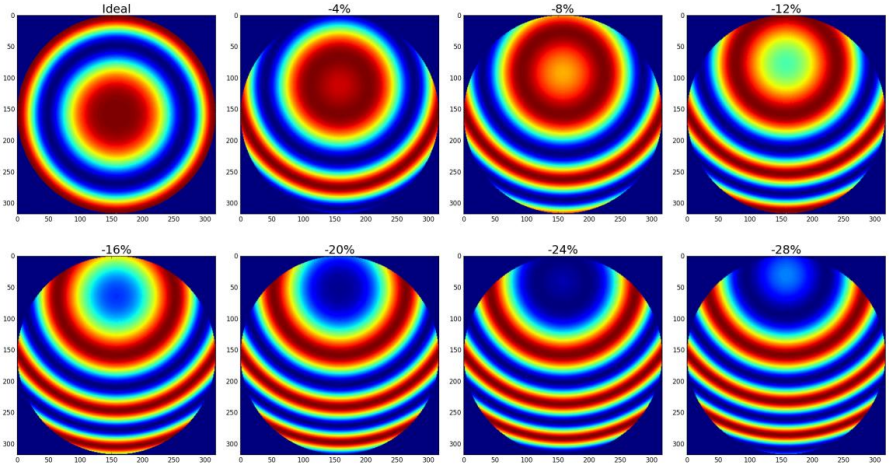

555
556 Fig.14. The Haidinger fringes at 1/2 maximum OPD (the maximum misalignment position) for Fig.
557 13
558

Atmos. Meas. Tech. Discuss., https://doi.org/10.5194/amt-2017-382
Manuscript under review for journal Atmos. Meas. Tech.
Discussion started: 10 January 2018

Atmospheric Measurement Techniques Discussions

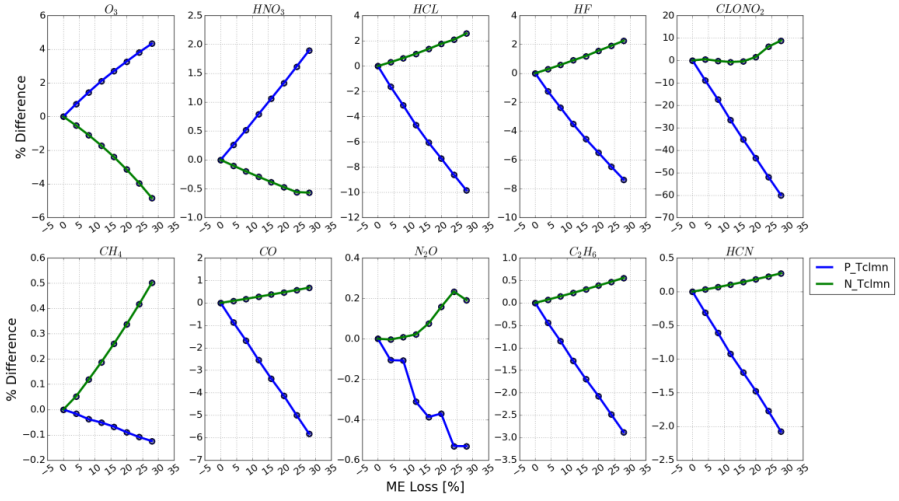

559

560 Fig.15. Sensitivity of total column with respect to ME deviation. "P_Tclmn" represents the
561 sensitivity of total column with respect to positive ME deviation and "N_Tclmn" represents the
562 sensitivity of total column with respect to negative ME deviation.

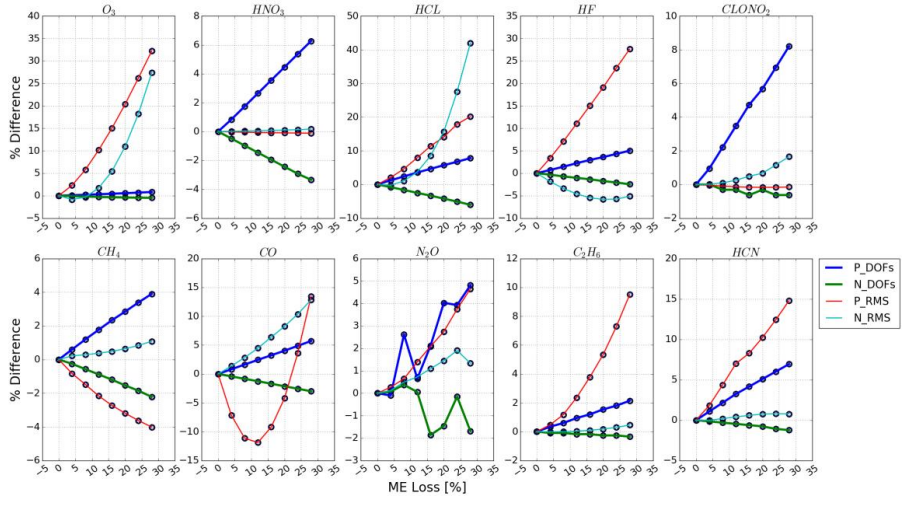

563

564 Fig.16. The same as Fig.15 but for DOFs and fitting RMS. The acronyms in the legend are similar
565 to those in Fig.15

Atmos. Meas. Tech. Discuss., https://doi.org/10.5194/amt-2017-382
Manuscript under review for journal Atmos. Meas. Tech.
Discussion started: 10 January 2018

Atmospheric Measurement Techniques Discussions

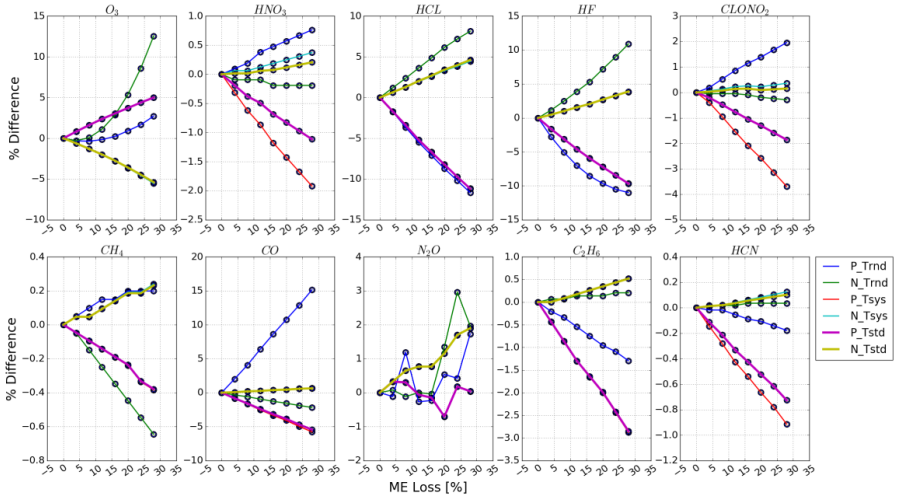

566

567 Fig.17. The same as Fig.15 but for total random uncertainty, total systematic uncertainty and total
568 uncertainty. The acronyms in the legend are similar to those in Fig.15. "Trnd", "Tsys" and "Tstd"
569 represent total random uncertainty, total systematic uncertainty and total uncertainty, respectively.

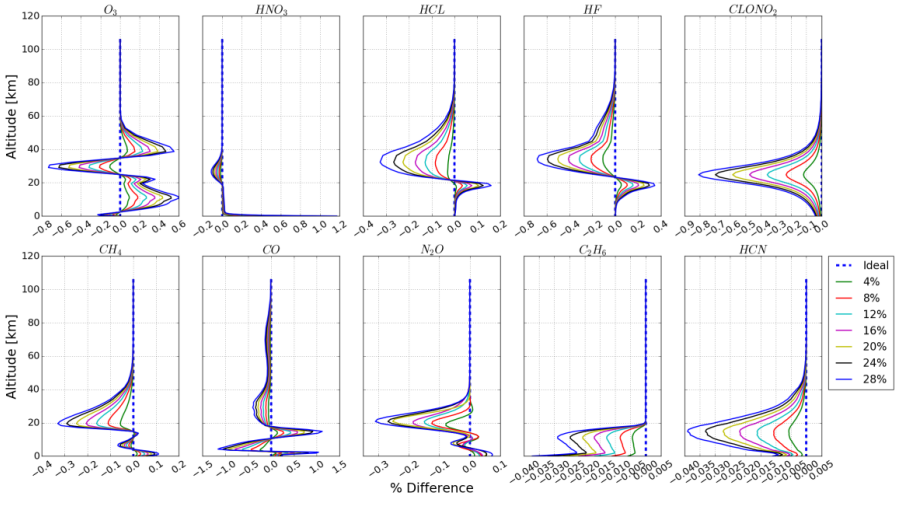

570

571 Fig.18. Sensitivity of profile with respect to ME deviation. "4%" represents the ME amplitude
572 deviation is 4%. The nomenclature for other plot labels is straightforward.

Atmos. Meas. Tech. Discuss., https://doi.org/10.5194/amt-2017-382
Manuscript under review for journal Atmos. Meas. Tech.
Discussion started: 10 January 2018

Atmospheric Measurement Techniques Discussions

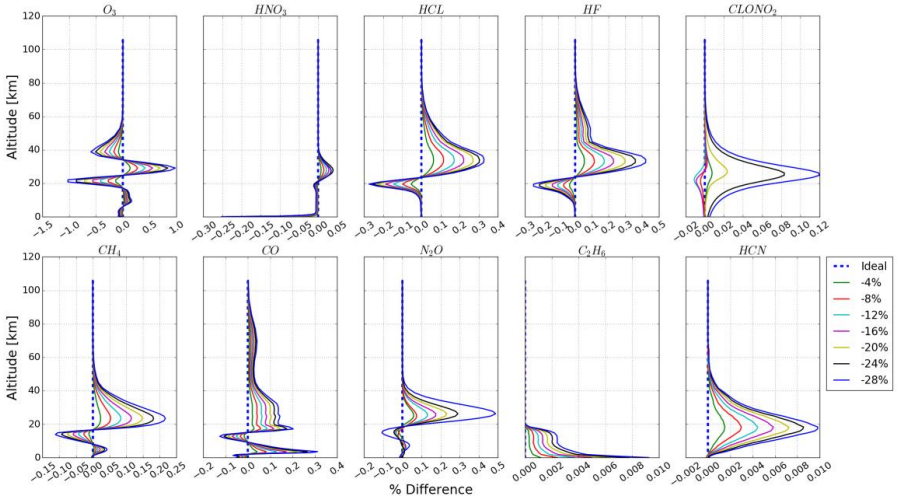

573
574 Fig.19. The same as Fig.18 but for negative ME deviation.

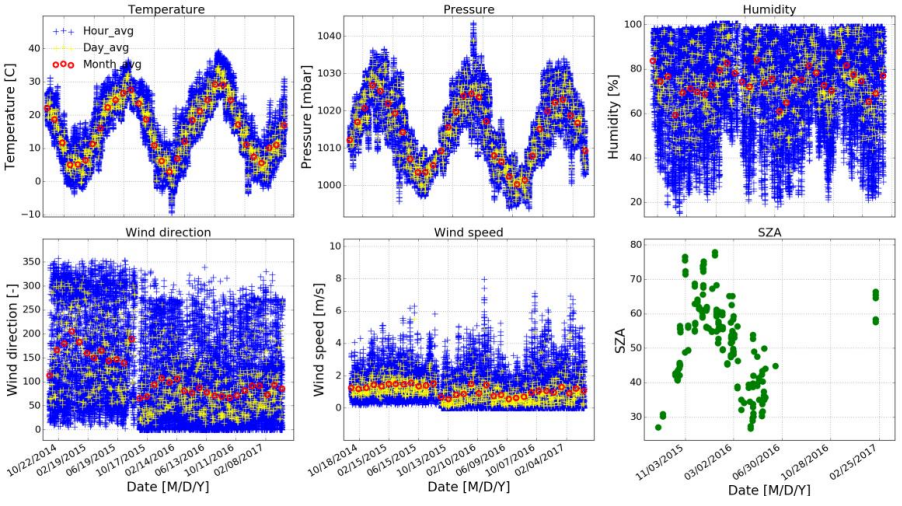

575
576 Fig.20. The meteorological data and SZAs record at Hefei from September 2014 to April 2017.
577 Large span of all these parameters are shown.

Atmos. Meas. Tech. Discuss., https://doi.org/10.5194/amt-2017-382
Manuscript under review for journal Atmos. Meas. Tech.
Discussion started: 10 January 2018

Atmospheric Measurement Techniques Discussions

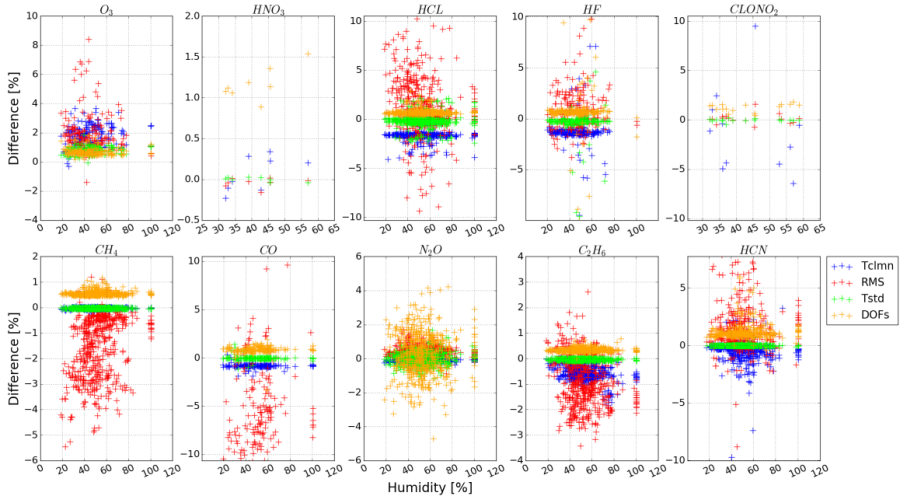

578
579
580 Fig.21. Fractional difference in total column, RMS, total uncertainty, and DOFs under different
581 humidity conditions from September 2014 to April 2017 for ILS *j* with a maximum ME deviation
582 of 5%.

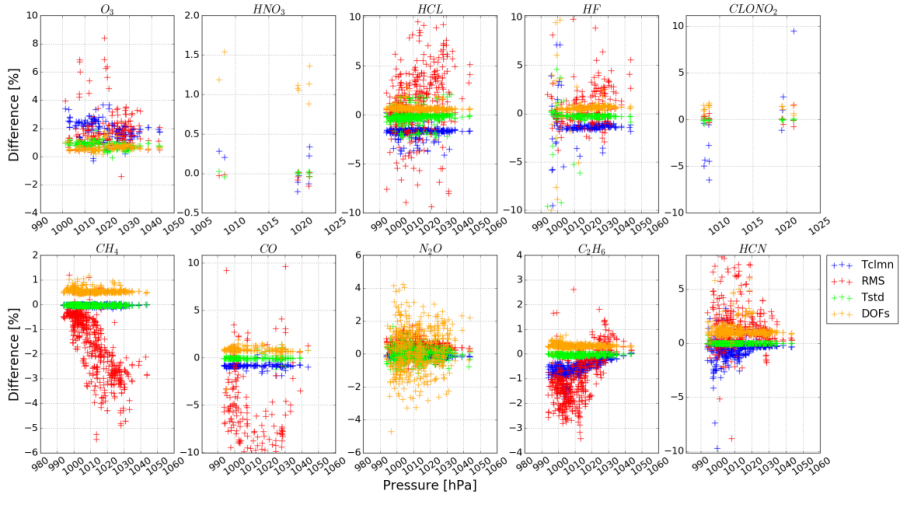

583
584 Fig.22. The same as Fig.21 but for surface pressure.

Atmos. Meas. Tech. Discuss., https://doi.org/10.5194/amt-2017-382
Manuscript under review for journal Atmos. Meas. Tech.
Discussion started: 10 January 2018

Atmospheric Measurement Techniques Discussions

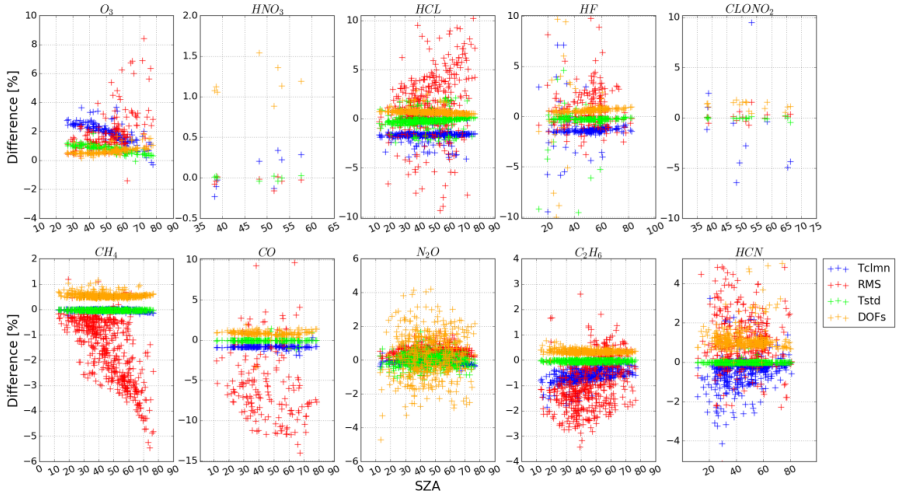

585
586 Fig.23. The same as Fig.21 but for SZA.

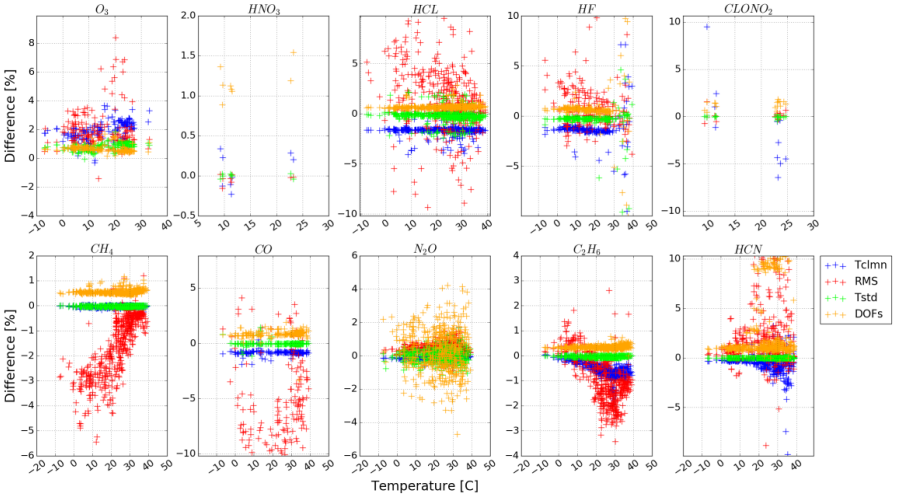

587
588 Fig.24. The same as Fig.21 but for surface temperature.

Atmos. Meas. Tech. Discuss., https://doi.org/10.5194/amt-2017-382
Manuscript under review for journal Atmos. Meas. Tech.
Discussion started: 10 January 2018

Atmospheric Measurement Techniques Discussions

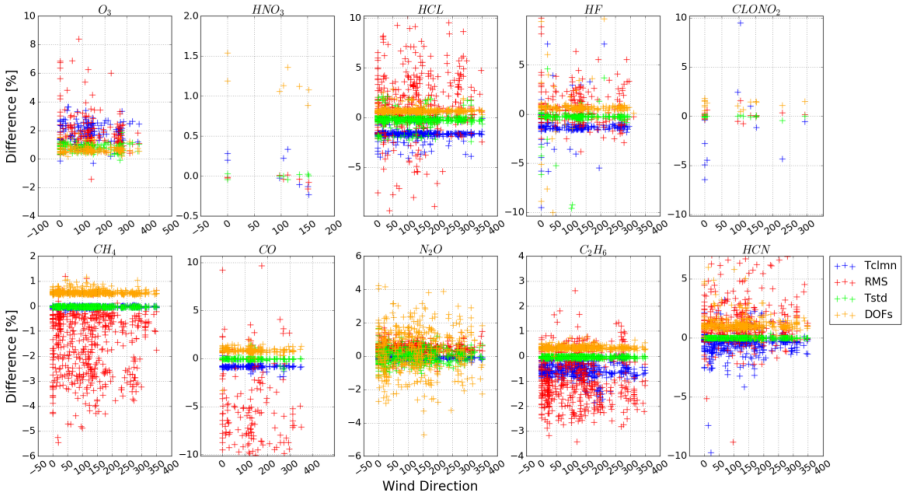

589

590 Fig.25. The same as Fig.21 but for wind direction.

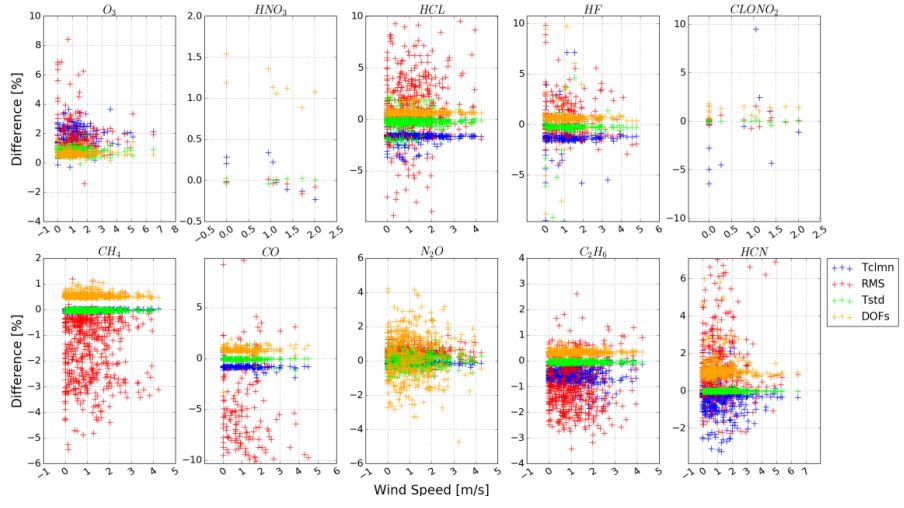

591

592 Fig.26. The same as Fig.21 but for wind speed

Atmos. Meas. Tech. Discuss., https://doi.org/10.5194/amt-2017-382
Manuscript under review for journal Atmos. Meas. Tech.
Discussion started: 10 January 2018

10 Tables

Table 1. Misalignments simulated in the ALIGN60

Type [a]	Description	Input [b]	Output in maximum
a	No misalignment occurs: interferometer in ideal condition	none	ME amplitude: 1.00 PE: 0.000 rad.
b	Decenter of entrance field stop defining FOV: causes a linear increase in misalignment along OPD	0.33 [mrad] field stop error	ME amplitude: 0.86 PE: -0.056rad.
c	Decenter of path measuring laser: causes a linear increase in phase error along OPD	0.33 [mrad] laser error	ME amplitude:1.00 PE: -0.152rad.
d	Constant shear: causes a constant shear offset of fixed retro-reflector	0.03 [cm]	ME amplitude: 1.00 PE: -0.056 rad.
e	Decreasing linear shear: causes a linear decrease in misalignment along OPD	0.03-0.00017*OPD [cm]	ME amplitude: 1.16 PE: -0.007 rad.
f	Increasing linear shear: causes a linear increase in misalignment along OPD	0.00017*OPD [cm]	ME amplitude: 0.86 PE: -0.056 rad.
g	Cosine bending of scanner bar: causes a cosine decrease in misalignment along OPD	0.03*cos(π*OPD/360) [cm]	ME amplitude: 1.16 PE: -0.013 rad.
h	Sine bending of scanner bar: causes a sine increase in misalignment along OPD	0.03*sin(π*OPD/360) [cm]	ME amplitude: 0.86 PE: -0.056 rad.
i	Cosine & sine bending of scanner bar: causes a chord increase in misalignment before 1/2 maximum OPD and causes a chord decrease in misalignment after 1/2 maximum OPD	0.073*(sin(π*OPD/360)+ cos(π*OPD/360))-0.073 [cm]	ME amplitude: 0.86 PE: -0.029 rad.
j	Constant shear plus cosine & sine bending of scanner bar: causes a chordal decrease in misalignment before 1/2 maximum OPD and causes a chordal increase in misalignment after 1/2 maximum OPD	-0.073*(sin(π*OPD/360)+ cos(π*OPD/360))+0.103 [cm]	ME amplitude: 1.16 PE: - 0.056 rad.

[a] The *b*, *f*, *h*, and *i* are referred to increasing misalignment, the *e*, *g*, and *j* are referred to decreasing misalignment

[b] The input control file (i.e., align60.inp) for ideal condition is attached in the supplement. The input files for other gases can be straight forward.

Atmos. Meas. Tech. Discuss., https://doi.org/10.5194/amt-2017-382
Manuscript under review for journal Atmos. Meas. Tech.
Discussion started: 10 January 2018

Atmospheric Measurement Techniques Discussions

Table 2. Summary of the retrieval parameters used for all NDACC gases. All micro windows (MW) are given in cm^{-1}

Gases		O_3	HNO_3	HCl	HF	$ClONO_2$	CH_4	CO	N_2O	C_2H_6	HCN
Retrieval code		SFIT4 v 0.9.4.4	SFIT4 v 0.9.4.4	SFIT4 v 0.9.4.4	SFIT4 v 0.9.4.4	SFIT4 v 0.9.4.4	SFIT4 v 0.9.4.4	SFIT4 v 0.9.4.4	SFIT4 v 0.9.4.4	SFIT4 v 0.9.4.4	SFIT4 v 0.9.4.4
Spectroscopy		HITRAN2008	HITRAN2008	HITRAN2008	HITRAN2008	HITRAN2008	HITRAN2008	HITRAN2008	HITRAN2008	HITRAN2008	HITRAN2008
P, T profiles		NCEP	NCEP	NCEP	NCEP	NCEP	NCEP	NCEP	NCEP	NCEP	NCEP
A priori profiles for target/interfering gases except H_2O		WACCM	WACCM	WACCM	WACCM	WACCM	WACCM	WACCM	WACCM	WACCM	WACCM
MW for profile retrievals		1000-1004.5	867.5-870	2727.73-2727.83 2775.7-2775.8 2925.8-2926.0	4109.4-4110.2	779.85-780.45 782.55-782.87	2613.7-2615.4 2835.5-2835.8 2921.0-2921.6	2057.7-2058 2069.56-2069.76 2157.5-2159.15	2441.8-2444.6 2481.2-2482.5	2976-2978 2982.6-2984.5	3268-3268.38 3287-3287.48
Retrieved interfering gases		H_2O, CO_2, C_2H_4, O3668, O3686	H_2O, OCS, NH_3	CH_4, NO_2, O_3, N_2O, HDO	H_2O, HDO, CH_4	O_3, HNO_3, H_2O, CO_2	CO_2, NO_2, H_2O, HDO	O_3, N_2O, CO_2, OCS, H_2O	CO_2, CH_4	H_2O, CH_4, O_3	H_2O, O_3, C_2H_2, CH_4
H_2O treatment	A priori profile	NCEP	NCEP	NCEP	NCEP	NCEP	NCEP	NCEP	NCEP	NCEP	NCEP
	Fit in each WM	Profile retrieval	Scaling retrieval only	Profile retrieval	Profile retrieval	Scaling retrieval only	Profile retrieval	Profile retrieval	Profile retrieval	Profile retrieval	Profile retrieval
SNR for de-weighting		None	None	300	None	None	None	500	None	None	None
Regularization	S_a	Diagonal: 20% No correlation	Diagonal: 50% No correlation	Diagonal: 50% No correlation	Diagonal: 10% No correlation	Diagonal: 100% Exponential correlation HWHM: 8 km	Diagonal: 10% No correlation	Diagonal: 11% ~ 27% No correlation	Diagonal: 10% No correlation	Diagonal: 10% No correlation	Diagonal: 21% ~ 79% No correlation
	SNR	Real SNR	Real SNR	Real SNR	Real SNR	Real SNR	Real SNR	Real SNR	Real SNR	Real SNR	Real SNR
ILS		ALIGN60	ALIGN60	ALIGN60	ALIGN60	ALIGN60	ALIGN60	ALIGN60	ALIGN60	ALIGN60	ALIGN60
Error analysis		Systematic error: -Smoothing error (smoothing) [a] -Errors from parameters not retrieved by sfit4 [b]: Background curvature (curvature), Optical path difference (max_opd), Field of view (omega), Solar line strength (solstrnth), Background slope (slope), Solar line shift (solshift), Phase (phase), Solar zenith angle(sza), Line temperature broadening (linetair_gas), Line pressure broadening (linepair_gas), Line intensity(lineint_gas) Random error: -Interference errors: retrieval parameters (retrieval_parameters), interfering species (interfering_species) -Measurement error (measurement) - Errors from parameters not retrieved by sfit4 [b]: Temperature (temperature), Zero level (zshift)									

[a] The bracket shows the corresponding acronym in Figs.5 and 6

[b] The input uncertainties of all these items are the same and are included into error analysis if they are not retrieved. Otherwise, the corresponding uncertainties wouldn't be included.

Atmos. Meas. Tech. Discuss., https://doi.org/10.5194/amt-2017-382
Manuscript under review for journal Atmos. Meas. Tech.
Discussion started: 10 January 2018

Table 3. Altitude ranges with sensitivity larger than 0.5 for all NDACC gases

Items	O_3	HNO_3	HCl	HF	$ClONO_2$	CH_4	CO	N_2O	C_2H_6	HCN
Altitude ranges (km)	Ground - 44	17 - 28	18 - 42	18-44	20 - 28	Ground - 31	Ground - 27	Ground - 31	Ground - 13.5	4.5-18
DOFs	5.2	1.4	1.5	1.3	0.55	3.5	3.8	4.0	1.2	1.1

Atmos. Meas. Tech. Discuss., https://doi.org/10.5194/amt-2017-382
Manuscript under review for journal Atmos. Meas. Tech.
Discussion started: 10 January 2018

Atmospheric Measurement Techniques Discussions

Table 4. The dominant sources of systematic errors and random errors for all NDACC gases

Items	O_3	HNO_3	HCl	HF	$ClONO_2$	CH_4	CO	N_2O	C_2H_6	HCN
Systematic error	smoothing error, line intensity, line pressure broadening	smoothing error	smoothing error	smoothing error, SZA line intensity, line pressure broadening	smoothing error	smoothing error, line pressure broadening, line intensity	smoothing error, line pressure broadening, curvature	smoothing error, line pressure broadening, line intensity	smoothing error, line pressure broadening	smoothing error, line pressure broadening, line intensity
Random error	measurement error, temperature,	measuremen t error	Measurement error, retrieval parameters, interfering species, temperature	measuremen t error, temperature,	measuremen t error	zero level, measuremen t error, temperature	zero level	measuremen t error, zero level, temperature	zero level, measuremen t error	measurement error, interfering species, retrieval parameters, zero level

Atmos. Meas. Tech. Discuss., https://doi.org/10.5194/amt-2017-382
Manuscript under review for journal Atmos. Meas. Tech.
Discussion started: 10 January 2018

Table 5. Recommendation for suppressing fractional difference in total column for $ClONO_2$ and other NDACC gases within 10% and 1%, respectively

Items	O_3	HNO_3	HCl	HF	$ClONO_2$	CH_4	CO	N_2O	C_2H_6	HCN
Positive ME	< 6%	<15%	<5%	<5%	<5%	*	<5%	*	< 9%	<13%
Negative ME	< 6%	*	<12%	<12%	*	*	*	*	*	*

*The influence on $ClONO_2$ is less than 10% and on all other NDACC gases are less than 1% even the ILS degrade by an excessively large of 28%, and thus can normally be regarded as negligible.